RESEARCH ARTICLE

Tribological mechanism of carbon group nanofluids on grinding interface under minimum quantity lubrication based on molecular dynamic simulation

Dexiang WANG[a], Yu ZHANG[a], Qiliang ZHAO[a], Jingliang JIANG[a], Guoliang LIU[a,b], Changhe LI (✉)[a]

[a] School of Mechanical and Automotive Engineering, Qingdao University of Technology, Qingdao 266520, China
[b] State Key Laboratory of High Performance Complex Manufacturing, Central South University, Changsha 410083, China
✉ Corresponding author. E-mail: sy_lichanghe@163.com (Changhe LI)

ABSTRACT Carbon group nanofluids can further improve the friction-reducing and anti-wear properties of minimum quantity lubrication (MQL). However, the formation mechanism of lubrication films generated by carbon group nanofluids on MQL grinding interfaces is not fully revealed due to lack of sufficient evidence. Here, molecular dynamic simulations for the abrasive grain/workpiece interface were conducted under nanofluid MQL, MQL, and dry grinding conditions. Three kinds of carbon group nanoparticles, i.e., nanodiamond (ND), carbon nanotube (CNT), and graphene nanosheet (GN), were taken as representative specimens. The [BMIM]BF$_4$ ionic liquid was used as base fluid. The materials used as workpiece and abrasive grain were the single-crystal Ni–Fe–Cr series of Ni-based alloy and single-crystal cubic boron nitride (CBN), respectively. Tangential grinding force was used to evaluate the lubrication performance under the grinding conditions. The abrasive grain/workpiece contact states under the different grinding conditions were compared to reveal the formation mechanism of the lubrication film. Investigations showed the formation of a boundary lubrication film on the abrasive grain/workpiece interface under the MQL condition, with the ionic liquid molecules absorbing in the groove-like fractures on the grain wear's flat face. The boundary lubrication film underwent a friction-reducing effect by reducing the abrasive grain/workpiece contact area. Under the nanofluid MQL condition, the carbon group nanoparticles further enhanced the tribological performance of the MQL technique that had benefited from their corresponding tribological behaviors on the abrasive grain/workpiece interface. The behaviors involved the rolling effect of ND, the rolling and sliding effects of CNT, and the interlayer shear effect of GN. Compared with the findings under the MQL condition, the tangential grinding forces could be further reduced by 8.5%, 12.0%, and 14.1% under the diamond, CNT, and graphene nanofluid MQL conditions, respectively.

KEYWORDS grinding, minimum quantity lubrication, carbon group nanofluid, tribological mechanism

1 Introduction

Effective cooling and lubrication in the grinding zone can greatly improve the surface integrity of the workpiece and prolong the service life of the grinding wheel. At present, flood cooling and lubrication is the most widely used technique in grinding. However, the flood technique is limited by high fluid usage cost [1], low usage flow rate [2], and high-risk threat to both human health and the environment [3], which contradicts the requirements of green manufacturing. New cooling and lubrication methods are needed to avoid the problems of the flood technique.

Minimum quantity lubrication (MQL) sprays an extremely small amount of grinding fluid to the grinding zone, and it is mixed and atomized with high-pressure air by using a high-pressure and high-speed aerosol jet to achieve cooling and lubrication. Compared with the flood technique, MQL can greatly reduce the fluid usage cost, improve the usage flow rate, and reduce the threat to both human health and the environment [4]. Furthermore, MQL can obtain better lubrication performance than the flood technique [5]. However, the heat transfer capability of MQL is insufficient, with the aerosol jet failing to

achieve the ideal cooling performance [6,7]. This situation can be explained by the total wetting area by all MQL spray droplets per unit time being only approximately 6% of the grinding wheel surface in the grinding zone [8]. Therefore, air is mainly involved in the heat exchange on the wheel/workpiece interface. However, the thermal conductivity of air is as low as 0.0259 W/(m·K) at room temperature [9], causing the convective heat transfer coefficient of the aerosol jet to be smaller than that of the flood technique by one to two orders of magnitude. The insufficient heat transfer capacity is a technical bottleneck restricting the wide application of MQL in grinding.

Nanofluid minimum quantity lubrication (NMQL) uses solid nanoparticles to participate in the heat exchange on the grinding wheel/workpiece interface [10]. The original intention is to strengthen the heat transfer capacity of MQL via the small size effect and large specific surface area of nanoparticles, thereafter increasing the heat conduction and convective heat transfer coefficient [11–13]. Further research has shown that NMQL not only can strengthen the heat transfer capacity but also improve the friction-reducing and anti-wear performance of MQL [14,15]. This feature suggests that introducing solid nanoparticles changes the formation mechanism of lubrication films and the friction-reducing and anti-wear performance on the MQL grinding interface. Revealing the tribological mechanism of nanofluids on the MQL grinding interface can provide theoretical support for optimizing the NMQL grinding process.

1.1　MQL grinding performance of carbon group nanofluids

At present, the widely used nanoparticles in NMQL grinding are as follows: metallic and nonmetallic compounds, such as Al_2O_3 [16], CuO [17], MoS_2 [18], and SiO_2 [19]; pure metals, such as Cu [20] and Ag [21]; and carbon group nanoparticles, such as carbon nanotubes (CNTs) [22–24], graphene nanosheets (GNs) [25], and nanodiamonds (NDs) [26]. Numerous studies have shown that carbon group nanofluids can achieve good cooling and lubrication performance on the MQL grinding interface.

1.1.1　Diamond nanofluid minimum quantity lubrication (DN-MQL)

Wang et al. [27] used palm oil as a base fluid to prepare nanofluids with six different kinds of nanoparticles, namely, ZrO_2, CNTs, NDs, MoS_2, SiO_2, and Al_2O_3. Grinding experiments of nickel-based alloy GH4169 under NMQL, MQL, and flood grinding conditions were conducted, and the lubrication performance under different cooling and lubrication conditions were

compared. Comparative results showed that CNT and diamond nanofluids can enhance the lubrication performance of the MQL technique when only pure palm oil was used. Lee et al. [28] used paraffin oil as the base fluid and Al_2O_3 and ND nanoparticles to prepare nanofluids. Grinding experiments were conducted under NMQL, MQL, and dry grinding conditions, and the sk-41C tool steel was used as a workpiece material. The influences of the particle size and volume fraction of nanoparticles on the lubrication performance were analyzed. Their analyses showed that diamond nanofluid minimum quantity lubrication (DN-MQL) can more significantly reduce the grinding force and improve the workpiece surface quality compared with MQL. Furthermore, the higher volume fraction and smaller particle size of the nanoparticles were more effective in reducing the grinding force. Shen et al. [29] prepared water-based nanofluids with Al_2O_3 and ND nanoparticles. The grinding performances were experimentally evaluated under dry, flood, MQL, and NMQL grinding conditions. The influence of the volume fraction of nanoparticles on the lubrication performance was also analyzed. Their evaluation showed that grinding force and workpiece surface roughness can be reduced under the DN-MQL condition compared with the flood grinding and MQL conditions, and the surface burn of the workpiece was also relieved. Moreover, the high-volume fraction of the nanoparticles was more beneficial for reducing grinding wheel wear.

1.1.2　Carbon nanotube nanofluid minimum quantity lubrication (CNT-MQL)

Kumar and Ghosh [30] prepared CNT nanofluids by using deionized water. Grinding experiments were conducted under flood, MQL, and NMQL grinding conditions, and AISI 52100 bearing steel was used as the workpiece material. The grinding performances were compared under different cooling and lubrication conditions. Force ratio, specific energy, G-ratio, and surface residual stress were used as evaluation indexes. According to the comparisons, carbon nanotube nanofluid minimum quantity lubrication (CNT-MQL) can obtain the minimum values of tangential force, force ratio, and specific energy and the maximum values of G-ratio and surface compressive residual stress. Huang et al. [31] prepared nanofluids by using Castrol Carecut ES1 cutting oil and CNTs. Under the dry, MQL, and NMQL grinding conditions, the grinding performances of NAK80 mold steel were evaluated using grinding force, grinding temperature, surface roughness, and surface morphology as the indexes. Their evaluation showed that using 0.25 wt.% of CNT nanofluid can more effectively reduce grinding force, grinding temperature, and surface roughness compared with using Castrol Carecut ES1

cutting oil only. Gao et al. [32] used palm oil as base fluid to prepare CNT nanofluids. A single-diamond grain was used to grind the carbon fiber-reinforced polymer (CFRP) workpiece under dry, MQL, and NMQL grinding conditions. Their experiments showed that CNT nanofluids can further improve the tribological performance on the grain/workpiece interface. The friction coefficient under MQL was 0.156, whereas it was only 0.141 under CNT-MQL.

1.1.3   Graphene nanofluid minimum quantity lubrication (GN-MQL)

Singh et al. [33] used olive oil, sunflower oil, and canola oil to prepare graphene nanofluids. The grinding performances of Ti–6Al–4V-ELI were experimentally studied under dry, flood, MQL, and GN-MQL grinding conditions. Specific energy, force ratio, surface roughness, grinding force, and grinding temperature were used as indexes. Their research showed the optimal weight concentration of GNs to be 1.5 wt.%, with surface roughness, normal force, specific energy, and force ratio reduced by 16.9%, 22.1%, 33.83%, and 15.1%, respectively, as opposed to those under flood grinding that used synthetic fluid. Li et al. [34] used GNs as additives of the LB2000 fluid to improve the grinding performance of TC4 alloy. The effects of the weight concentration of GNs on grinding force, grinding temperature, specific energy, and surface quality were analyzed. Their analyses showed the optimal weight concentration of GNs to be 0.1 wt.%, and the cooling and lubrication performance of MQL was effectively improved under this condition. De Oliveira et al. [35] used semi-synthetic emulsion to prepare graphene nanofluids. The grinding performances of Inconel 718 under the dry, flood, MQL, and NMQL grinding conditions were also studied. Their results showed that the 0.05 wt.% graphene nanofluid can attain the best grinding performance among all of the cooling and lubrication conditions.

The investigations mentioned above showed that carbon group nanofluids can achieve good lubrication performance on the MQL grinding interface while further improving the friction-reducing and anti-wear performances of the MQL technique.

1.2   Tribological mechanisms of carbon group nanoparticles on the MQL grinding interface

The academic world has proposed the following four effects to reveal the friction-reducing and anti-wear mechanisms of carbon group nanoparticles on the MQL grinding interface [36].

(1) Rolling effect. Nanoparticles transform sliding friction into rolling friction on the abrasive grain/workpiece interface (Fig. 1(a)).

(2) Filling effect. Nanoparticles are filled in the groove-like fractures on the workpiece surface where the repair of the workpiece surface occurs (Fig. 1(b)).

(3) Polishing effect. Nanoparticles play a polishing role on the abrasive grain/workpiece interface (Fig. 1(c)).

(4) Film effect. Chemical reaction films form on the abrasive grain/workpiece interface because of the chemical reaction of nanofluid, grain, and workpiece materials, while friction adsorption films form because of the tribological behaviors, such as adsorption, extrusion, shear, and deformation, of nanoparticles (Fig. 1(d)).

The tribological mechanisms proposed above were mainly speculated based on the image analyses of post-grinding surfaces of both the workpiece and grinding wheel by using a scanning electron microscope (SEM), atomic force microscope, and energy dispersive spectrometer (EDS). However, the interactions among abrasive grain, workpiece, and spray droplets on the MQL grinding interface are difficult to observe directly. Although the image analyses can explain some experimental phenomena, direct evidence for revealing the internal mechanisms are lacking. The formation mechanism of the lubrication film generated by the carbon group nanofluids on the MQL grinding interface
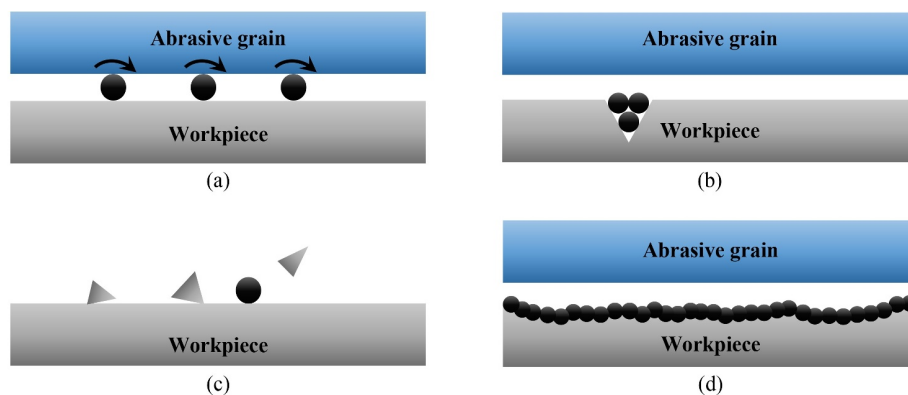
Fig. 1   Tribological behaviors of nanoparticles on the abrasive grain/workpiece interface: (a) rolling effect, (b) filling effect, (c) polishing effect, and (d) film effect.

must be explored to further reveal the friction-reducing and anti-wear mechanisms of carbon group nanoparticles.

1.3 Applications of molecular dynamic simulation in grinding

Molecular dynamic simulation can be used to perform microscale investigations, and it has been widely used to investigate the nano-grinding mechanisms and the evolution of crystal defects.

Ren et al. [37] conducted a molecular dynamics research on the ultra-high speed grinding characteristics of the single-crystal nickel. The evolutions of chip morphology, grinding force, and specific energy at different grinding stages were analyzed, and the quantitative relationship between subsurface defects and tangential force was revealed. Doan et al. [38] investigated the grinding mechanism of polycrystalline Ni–Fe–Co alloy via molecular dynamic simulation, and the important factors affecting the grinding mechanism were revealed. Peng et al. [39] investigated the adsorption synergy of multi-walled carbon nanotubes (MWCNTs) and MoS_2 mixed nanofluids via molecular dynamic simulation and further studied its influence on surface integrity in internal cooling grinding. Their simulation showed that MWCNTs and MoS_2 mixed nanoparticles could form a pressure-bearing sandwich structure to synergistically enhance the heat transfer and lubrication abilities of the base liquid. Wang et al. [40] conducted molecular dynamic simulations to study the cooling and lubrication effects on the MQL grinding interface. The generation and transfer mechanisms of grinding heat were revealed, and the evolutions of grinding force, force ratio, and liquid film between the abrasive grain and workpiece were analyzed.

The abovementioned studies indicate that molecular dynamic simulation is an effective method for microscale investigation. It can also reveal the tribological mechanisms of carbon group nanofluids on the MQL grinding interface at the atomic scale.

In summary, the participation of carbon group nanoparticles, represented by NDs, CNTs, and GNs, in the cooling and lubrication on the MQL grinding interface can further improve the friction-reducing and anti-wear properties of the MQL technique. However, the formation mechanism of the lubrication film generated by the carbon group nanofluids is not fully revealed and even needs sufficient evidence. In this research, molecular dynamic simulations were performed to explore the interactions on the abrasive grain/workpiece interface and reveal the formation mechanism of the lubrication film. Three representative kinds of carbon group nanoparticles, i.e., ND, CNT, and GN, were taken as research targets, and [BMIM]BF_4 ionic liquid was used as the base fluid of nanofluids. This research attempts to first disclose the formation mechanism of the lubrication film under the MQL condition in which only ionic liquid is used. Then, the tribological behaviors of the nanoparticles on the abrasive grain/workpiece interface are further investigated to reveal the tribological mechanisms of the carbon group nanofluids on the MQL grinding interface.

2 Molecular dynamics model for carbon group nanofluid MQL grinding

The molecular dynamic simulations were implemented in LAMMPS, and the simulations were visualized in OVITO (Open Visualization Tool). The establishment scheme of the molecular dynamics model for carbon group nanofluid MQL grinding is shown in Fig. 2.

2.1 Establishment of geometric models

2.1.1 Workpiece

The establishment of the workpiece model can be briefly described as follows. Single-crystal Ni–Fe–Cr series of
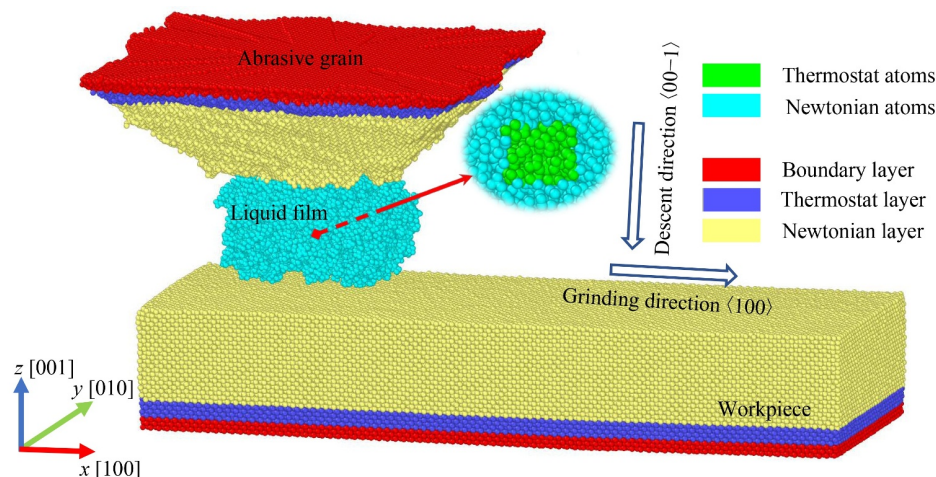
Fig. 2 Molecular dynamics model for the abrasive grain/workpiece interface.

Ni-based alloy was used as workpiece material, as it possesses a face-centered cubic structure with a lattice constant of 0.352 nm [41]. The geometric model of the workpiece was directly established with the Lattice command in LAMMPS. The workpiece material was selected as the simplified model of the Ni–Fe–Cr three-component alloy. The portions of Ni, Fe, and Cr atoms are 52%, 30%, and 18%, respectively, and the three elements were randomly distributed in the workpiece [41]. The size of the workpiece was 30 nm × 11 nm × 5 nm (Fig. 3). The whole workpiece model was successively divided into boundary, thermostat, and newton layers along the positive direction of the z axis (Fig. 2). The thicknesses of the boundary and thermostat layers were both 0.5 nm [41]. The boundary layer prevents the overall movement of the workpiece. The thermostat layer transfers grinding heat in time, avoiding the collapse of the simulation system that may be caused by high temperature. The newton layer atoms participate in the grinding process.

2.1.2 Abrasive grain

Single-crystal CBN was used as the abrasive grain material, as it possesses diamond-like structure with a lattice constant of 0.362 nm [41]. An optical microscope

was used to observe the surface of the electroplated CBN grinding wheel. The side faces of the CBN grain were uneven, and the grain wear's flat face had groove-like fractures (Fig. 4(a)). Therefore, the side faces of the abrasive grain were modeled to be uneven, and the wear's flat face was modeled with groove-like fractures.

The establishment of the abrasive grain model can be briefly described as follows. First, by using 3D MAX, the abrasive grain was established to have a quadrangular frustum pyramid shape. The side lengths of the bottom and top faces were 8 and 17 nm, respectively, and the height was 5 nm (Fig. 4(b)). Second, the side and bottom faces were made uneven via the noise function in 3D MAX, and then the abrasive grain model was exported and saved as an STL format file (Fig. 4(c)). Finally, the STL format model was transformed into LAMMPS data format by using Atomsk (Fig. 4(d)). Similar to the workpiece model, the abrasive grain model was divided into the boundary, thermostat, and newton layers along the −z direction. The thicknesses of the boundary and thermostat layers were both 0.5 nm (Fig. 2).

2.1.3 Nanofluids

(1) CNT
First, the (3,3) armchair single-walled CNT model was
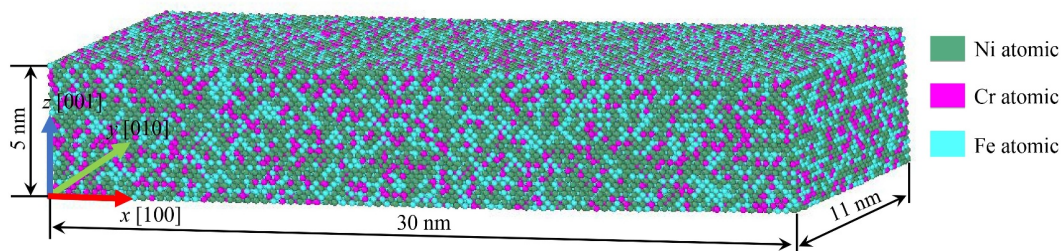
Fig. 3 Ni–Fe–Cr series of Ni-based alloy workpiece model.
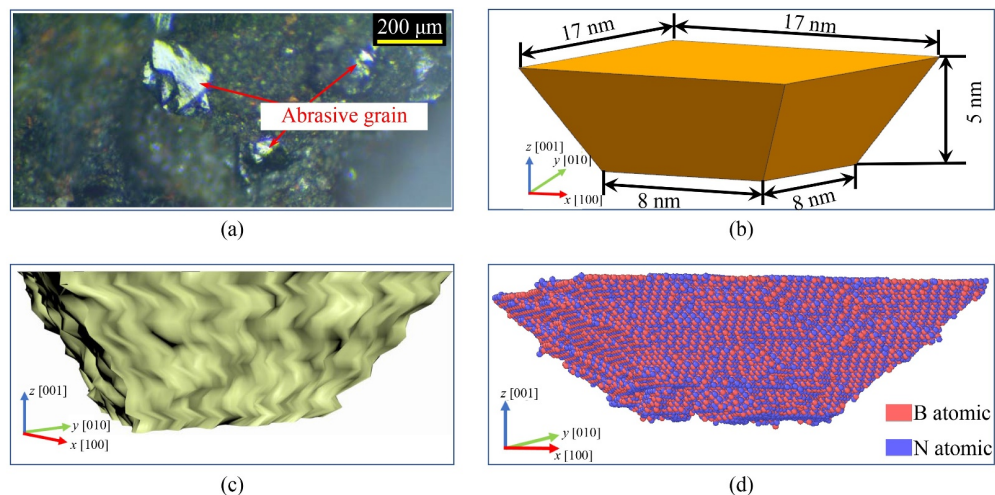
Fig. 4 Abrasive grain modeling process: (a) optical microscope image, (b) shape and dimension of the abrasive grain model, (c) noise treatment for the abrasive grain model, and (d) data format of the abrasive grain model.

established in Materials Studio, with length and diameter of 5.288 and 0.407 nm, respectively. The model was exported and saved as a CIF format file. Then, the CIF format model was converted to LAMMPS data format. The structure is shown in Fig. 5(a).

(2) ND

First, the diamond lattice structure was established in Materials Studio and exported and saved as a CIF format file. Then, the ND model was established using Atomsk via the subsequent supercell expansion and model cutting procedures. The diameter of the ND model was 1 nm. The structure is shown in Fig. 5(b).

(3) GN

First, the lattice cell of the single-layer GN was established using the Lattice command in LAMMPS. Then, the ABA stacked graphene sheet was constructed with three layers, with length of 3 nm and width of 3 nm. The interlayer spacing was 0.335 nm. The structure is shown in Fig. 5(c).

(4) Ionic liquid

First, the molecular structure of the [BMIM]BF$_4$ ionic liquid was established using Gaussian View 5.0, and then the optimal configuration of the [BMIM]BF$_4$ molecule was obtained from quantum chemical calculations in Gaussian 09 (Fig. 6(a)). Second, the ionic liquid molecule was used to generate 500 pairs of anions and cations in Packmol, which were randomly distributed in an 8 nm × 8 nm × 6 nm simulation box to form the liquid film. Then, the position information of all atoms was exported and saved as an XYZ format file. Finally, the XYZ format file was converted to Moltemplate data format. The details are shown in Fig. 6(b).

(5) Carbon group nanofluids

Three kinds of carbon group nanofluids, i.e., the diamond, CNT, and graphene nanofluids, were modeled. The amount of [BMIM]BF$_4$ molecules in the model was 500, and the amounts of the ND, CNT, and GN were all 1 (Fig. 7). The blue atoms in the figure belong to nanoparticles, and the green atoms belong to [BMIM]BF$_4$ ionic liquid.

Here, the establishment of the models is described by taking the CNT nanofluid as an example. First, the 500

(a)   (b)   (c)
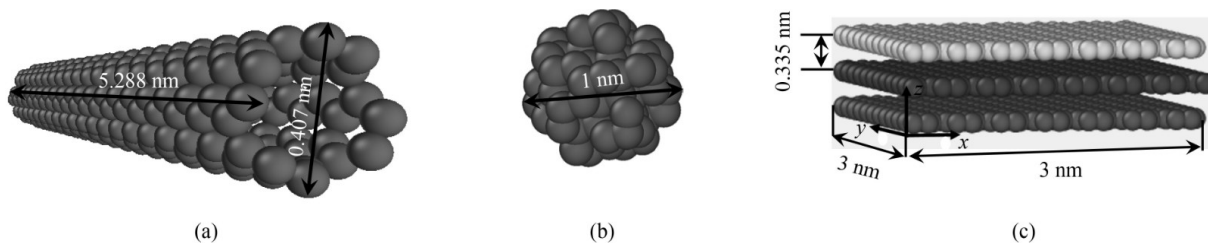
Fig. 5   Models of carbon group nanoparticles: (a) CNT; (b) ND; (c) GN.

(a)   (b)
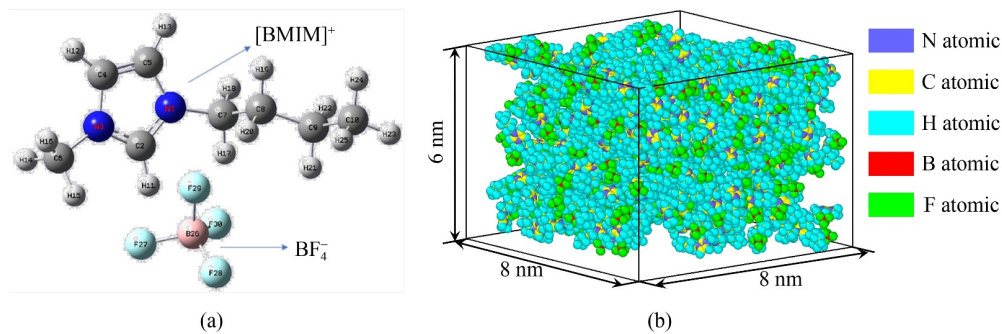
Fig. 6   Ionic liquid model: (a) optimal configuration of the [BMIM]BF$_4$ molecule and (b) liquid film.

(a)   (b)   (c)
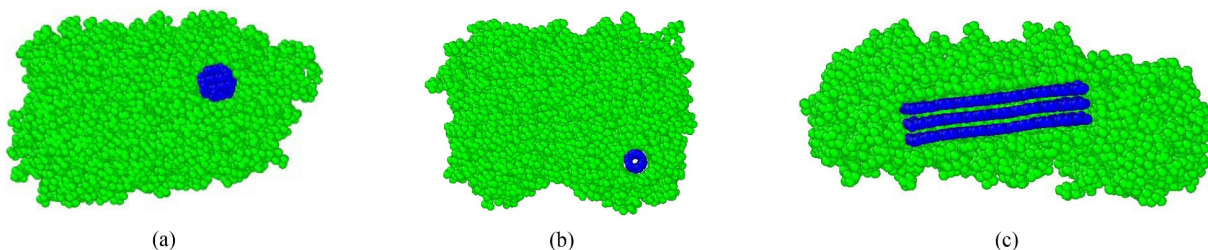
Fig. 7   Models of nanofluids: (a) diamond nanofluid, (b) CNT nanofluid, and (c) graphene nanofluid.

[BMIM]BF$_4$ molecules and the modeled CNT were randomly mixed in an 8 nm × 8 nm × 6 nm simulation box via Packmol to form the liquid film. Then, the position information of all atoms was exported and saved as an XYZ format file. Finally, the XYZ format model was converted to LAMMPS data format.

The nanofluid liquid film was divided into thermostat and newton layers (Fig. 2). The square-shaped thermostat layer had a side length of 1 nm, and its inner center was consistent with that of the liquid film. The remaining atoms all belonged to the newton layer.

2.2 Simulation details

Apart from simulations under the NMQL condition, simulations under the MQL and dry grinding conditions

were also performed. These simulations were used as reference for subsequent comparative analyses. The length and height directions of the workpiece, i.e., x and z directions, both had fixed boundaries. The width direction, i.e., y direction, was set as a periodic boundary. Each simulation could be divided into three stages: relaxation, descent, and grinding (Fig. 8).

(1) Relaxation stage

First, the workpiece, abrasive grain, and liquid film models were relaxed to their equilibrium states under the canonical ensemble by using a Berendsen thermostat as a means of controlling the system temperature at 298 K. The time length of the relaxation was 0.16 ns. The dry grinding condition would not need a liquid film. Under the conditions of MQL and NMQL, the liquid films were formed from the ionic liquid and nanofluids, respectively.
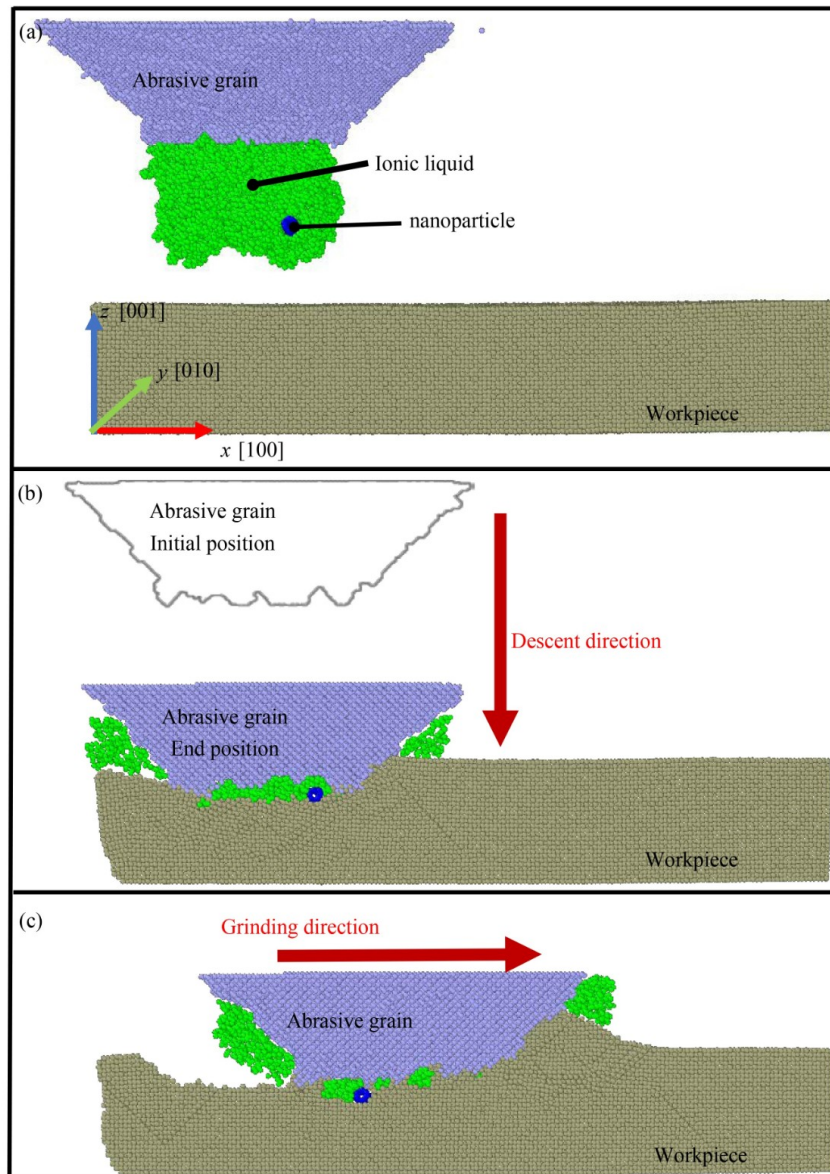
Fig. 8 Three simulation stages: (a) relaxation stage, (b) descent stage, and (c) grinding stage.

Then, the relaxed models were used to construct the simulation system. The conjugate gradient method was used to perform energy minimization for the simulation system. In this manner, overlaps in the positions of the atoms could be avoided. Finally, the whole simulation system was relaxed to its equilibrium state under the canonical ensemble by using a Berendsen thermostat to control the system temperature at 298 K. The time length of the relaxation was 0.16 ns.

(2) Descent stage

Under the microcanonical ensemble, the abrasive grain would descend and penetrate into the workpiece at the speed of 50 m/s along the $-z$ direction. The maximum penetration depth was 1.5 nm. A Nose–Hoover thermostat was used to control the thermostat layers of the abrasive grain, workpiece, and liquid film at 298 K. After the descent was completed, the Nose–Hoover thermostat was continually used to relax the whole simulation system to a new equilibrium state and eliminate the influence of the abrasive grain inertia on the penetration depth. The relaxation time was 0.03 ns.

(3) Grinding stage

Under the microcanonical ensemble, the Nose–Hoover thermostat was continually used to control the temperature of the thermostat layers at 298 K. The abrasive grain was disposed to grind the workpiece at the speed of 50 m/s along the x direction. The total grinding distance was 7.5 nm, and the time length was 0.15 ns.

All of the time steps in each simulation stage were set to 1 fs.

2.3 Potential functions

Potential functions were used to describe the intra/ intermolecular atomic scale interactions. Precision was regarded as an important parameter for ensuring the accuracy of the molecular dynamic simulation.

2.3.1 Abrasive grain

The interaction between B and N atoms in the CBN grain were described using the extended Tersoff potential function [42]; the selected parameter values can be obtained from Ref. [42]. The extended Tersoff potential function had been integrated into LAMMPS and could be invoked directly.

2.3.2 Workpiece

The interactions between atoms in the workpiece was expressed as an EAM potential function [43] as follows:

$$E(r_{ij}) = \frac{1}{2} \sum_{1 \leqslant j \neq i \leqslant N} R_{t_i t_j}(r_{ij}) + \sum_{i=1}^{N} F_{t_i}(\rho_i), \quad (1)$$

where E is the total energy, r_{ij} is the distance between atoms i and j, N represents the total amount of atoms in the system, R represents the pair interactions, F is the embedding energy, ρ_i is the local electron density around atom i, and t_i denotes the chemical species (Fe, Ni, or Cr). The selected parameter values in the EAM potential function can be obtained from Ref. [43].

2.3.3 Ionic liquid

The all-atom force field was used to describe intra/ intermolecular atomic-scale interactions in the [BMIM]BF$_4$ ionic liquid, a method developed by Liu et al. [44]. The all-atom force field is given by

$$E = \sum_{bonds} K_r (r - r_0)^2 + \sum_{angles} K_\theta (\theta - \theta_0)^2$$

$$+ \sum_{dihedrals} \frac{K_\phi}{2} [1 + \cos(n\phi - \gamma)]$$

$$+ \sum_{i<j} \left\{ 4\varepsilon_{ij} \left[\left(\frac{\sigma_{ij}}{r_{ij}} \right)^{12} - \left(\frac{\sigma_{ij}}{r_{ij}} \right)^6 \right] \right\} + \sum_{i<j} \frac{q_i q_j}{r_{ij}}, \quad (2)$$

$$\varepsilon_{ij} = \sqrt{\varepsilon_{ii}\varepsilon_{jj}}, \ \sigma_{ij} = (\sigma_{ii} + \sigma_{jj})/2. \quad (3)$$

The first term in Eq. (2) is the bond-stretching potential, where K_r is the bond-stretching energy coefficient, r represents the bond length, and r_0 is the equilibrium bond length. The second term is the bond angle-bending potential, where K_θ is the bond angle-bending energy coefficient, θ represents the bond angle, and θ_0 is the equilibrium bond angle. The third term is the torsional (dihedral) potential, where K_ϕ is the torsion energy coefficient, n is the multiphase factor, and γ is the equilibrium dihedral angle. The fourth term is the van der Waals potential in the Lennard–Jones (LJ) in 6–12 form, where ε_{ij} is the traditional well-depth, and σ_{ij} is the distance between atoms i and j, at which the energy of the two atoms reaches zero and minimum, respectively. The LJ parameters for dissimilar atoms were obtained from the Lorentz–Berthelot combination rule, as expressed in Eq. (3). The fifth term is the electrostatic potential, where q_i and q_j denote the electrical charge of atoms i and j, respectively. The selected values of the parameters in the all-atom force field can be obtained from Ref. [44].

2.3.4 Nanoparticles

The intralayer interactions in GNs were described using the Tersoff potential function [45], which could be integrated into LAMMPS and invoked directly. The interlayer interactions in the GNs were described using the LJ potential function, which is expressed as

$$E(r_{ij}) = 4\varepsilon_{ij} \left[\left(\frac{\sigma_{ij}}{r_{ij}} \right)^{12} - \left(\frac{\sigma_{ij}}{r_{ij}} \right)^6 \right]. \quad (4)$$

For the interlayer C–C interaction [46], the values of ε_{ij} and σ_{ij} were set to 2.964 meV and 3.407 Å, respectively, and the cutoff radius was 10 Å. The C–C interactions in CNTs and NDs were described using the Tersoff potential function. The selected parameters were the same as those for the interlayer interactions in GNs.

2.3.5 Interactions among abrasive grain, workpiece, and nanofluids

The interactions between abrasive grain and the workpiece were described using the Morse potential function [47]. The remaining interactions, i.e., among the abrasive grain, workpiece, and nanofluids, were all described using the LJ potential function.

The Morse potential function can be expressed as

$$E = D[e^{-2\alpha(r-r_0)} - 2e^{-\alpha(r-r_0)}], \qquad (5)$$

where D is the binding energy coefficient, and α is the gradient coefficient of the potential energy curve. The selected Morse potential function parameters are listed in Table 1.

The LJ parameters are listed in Tables 2 and 3. All parameters were obtained from the UFF force field model [48]. The cutoff radius was 15 Å.

Table 1 Morse potential function parameters. Reprinted with permission from Ref. [41] from Elsevier

Workpiece	Abrasive grain	D/eV	α/Å^{-1}	r_0/Å
Ni	N	1.5500	2.160	1.8600
	B	1.1220	1.340	2.1310
Fe	N	1.5400	2.144	1.8770
	B	1.1175	1.324	1.6339
Cr	N	1.5880	2.240	1.8520
	B	1.1490	1.416	1.6224

Table 2 LJ parameters for the interaction between carbon nanoparticle atoms and the remaining atoms

Nanoparticle	Workpiece	Abrasive grain	Ionic liquid	ε/eV	σ/Å
C		B		0.0059616	3.5342
C		N		0.0036910	3.3459
C	Ni			0.0017210	2.9778
C	Fe			0.0017210	3.0620
C	Cr			0.0016021	3.0126
C			N	0.0036910	3.3458
C			C	0.0045532	3.4309
C			H	0.0029475	3.0010
C			B	0.0059616	3.5342
C			F	0.0031420	3.2139

Table 3 LJ parameters for the interaction between ionic liquid atoms and the remaining atoms except the carbon nanoparticle

Ionic liquid	Workpiece	Abrasive grain	ε/eV	σ/Å
N	Ni		0.0013951	2.8927
	Fe		0.0013951	2.9769
	Cr		0.0012988	2.9275
		B	0.0048327	3.4491
		N	0.0029921	3.2607
C	Ni		0.0017210	2.9778
	Fe		0.0017210	3.0620
	Cr		0.0016021	3.0126
		B	0.0059616	3.5342
		N	0.0036910	3.3458
H	Ni		0.0011140	2.5480
	Fe		0.0011140	2.6322
	Cr		0.0010371	2.5827
		B	0.0038592	3.1043
		N	0.0023894	2.9159
B	Ni		0.0022533	3.0812
	Fe		0.0022533	3.1654
	Cr		0.0020977	3.1159
		B	0.0078055	3.6375
		N	0.0048327	3.4491
F	Ni		0.0011876	2.7609
	Fe		0.0011876	2.8451
	Cr		0.0011056	2.7956
		B	0.0041139	3.3173
		N	0.0025471	3.1288

2.4 Calculation methods of grinding force and stress distribution

Details of the calculation methods of grinding force and stress distribution can be referred from Ref. [49]. The method can be described briefly as follows. The tangential grinding force is calculated using the calculate reduce command in LAMMPS, and it is obtained from calculating the forces in the x, y, and z directions of the abrasive grain.

The calculation process of stress distribution can be divided into the following three parts: (1) Calculating the per-atom stress tensor for each atom in the simulation system: The tensor for each atom is stored as a six-element vector in the following order: σ'_x, σ'_y, σ'_z, τ'_{xy}, τ'_{xz}, and τ'_{yz}. (2) Scanning all atoms in the simulation system and calculating the macroscopic stress tensor at each atom according to Eq. (6): The macroscopic stress tensor of each atom is stored as a six-element vector in the following order: σ_x, σ_y, σ_z, τ_{xy}, τ_{xz}, and τ_{yz}. It can be obtained by accumulating the stress components of all

atoms within the sphere centered by the scanned atom and then dividing it by the volume of the sphere. The radius of the sphere is set to 1 nm. (3) Calculating the von Mises equivalent stress at each atom, σ_v, according to Eq. (7).

$$
\begin{cases}
\sigma_x = \sigma'_x/V = \sum_{i=1}^{N} \sigma'_{xi}/V, \\[2mm]
\sigma_y = \sigma'_y/V = \sum_{i=1}^{N} \sigma'_{yi}/V, \\[2mm]
\sigma_z = \sigma'_z/V = \sum_{i=1}^{N} \sigma'_{zi}/V, \\[2mm]
\tau_{xy} = \tau'_{xy}/V = \sum_{i=1}^{N} \tau'_{xyi}/V, \\[2mm]
\tau_{xz} = \tau'_{xz}/V = \sum_{i=1}^{N} \tau'_{xzi}/V, \\[2mm]
\tau_{yz} = \tau'_{yz}/V = \sum_{i=1}^{N} \tau'_{yzi}/V,
\end{cases}
\tag{6}
$$

$$
\sigma_v = \frac{1}{\sqrt{2}}\Big[(\sigma_x - \sigma_y)^2 + (\sigma_x - \sigma_z)^2 + (\sigma_z - \sigma_x)^2 \\
+ 6\big(\tau_{xy}^2 + \tau_{yz}^2 + \tau_{zx}^2\big)\Big]^{1/2},
\tag{7}
$$

where V is the volume of the sphere.

3 Molecular dynamic simulations for carbon group nanofluid MQL grinding

3.1 Analyses of tangential grinding force

Tangential grinding force is used to evaluate the lubrication performance on the abrasive grain/workpiece interface under the NMQL, MQL, and dry grinding conditions. The simulations are plotted in Fig. 9(a). The tangential forces tend to gradually stabilize when the grinding distance exceeds 1 nm. Therefore, the average forces within the distance range of 1–7.5 nm are used for subsequent analyses. The results are shown in Fig. 9(b). Under the MQL condition, the tangential force is reduced by 16.9% in contrast to that under dry grinding. Under the NMQL condition, the tangential force is further reduced. Compared with the findings under the MQL condition, the tangential forces decrease by 12.0%, 8.5%, and 14.1% under the CNT-MQL, DN-MQL, and GN-MQL conditions, respectively.

Similar qualitative laws have also been obtained from the experimental data in the literature [27,28,31,33,34, 50–53], thus proving the correctness of the molecular dynamic simulations. Lee et al. [28] and Yuan et al. [50] showed that the tangential force under the DN-MQL condition could be further reduced compared with that under the MQL condition (Figs. 10(a) and 10(b)). The grinding experiment of Inconel 718 by Jia et al. [51] showed that the tangential grinding force under the DN-MQL condition decreased by 20.28% compared with that under the MQL condition (Fig. 10(c)). Wang et al. [27] found that the tangential grinding force under the CNT-MQL and DN-MQL conditions could be reduced by 4.8% and 14.15%, respectively, in contrast to that under pure palm oil MQL condition (Fig. 10(d)). Huang et al. [31] found that CNT-MQL could further reduce the tangential force compared with MQL, with a maximum reduction of 37.16% (Fig. 10(e)). The grinding experiment of Inconel 718 under the GN-MQL condition by Pavan et al. [52] showed that tangential grinding force decreased by 27.22% in contrast to that under the MQL condition (Fig. 10(f)). Li et al. [34] reported that when GN was used for the TC4 alloy under the NMQL condition, the tangential grinding force could be reduced by up to
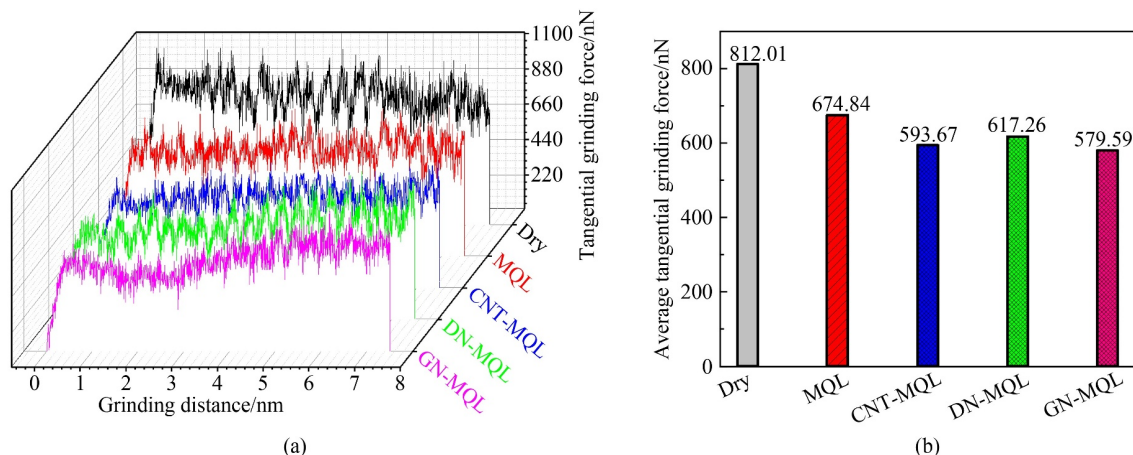
Fig. 9 Molecular dynamic simulations of tangential grinding forces: (a) histories of tangential grinding forces under different conditions, and (b) average tangential grinding forces under different conditions.

42.8% in contrast to that under MQL condition (Fig. 10(g)). Singh et al. [33] performed grinding experiments of Ti–6Al–4V and determined that, compared with pure vegetable oil in MQL grinding, the tangential grinding force under the GN-MQL condition could decrease by up to 26.71% (Fig. 10(h)). Ibrahim et al. [53] found that the tangential grinding force under the GN-MQL condition could be reduced by up to 79.1% in contrast to that using pure palm oil only (Fig. 10(i)).

Molecular dynamic simulation, given its limitations, can only implement nanoscale investigations of the abrasive grain/workpiece interface, but the interface is at the micrometer scale. Differences in the research scales have resulted in simulations being a few orders of magnitude smaller than the experimental tangential forces. However, our simulations can still obtain similar qualitative laws as those in the published papers mentioned above. According to the qualitative laws, carbon group nanofluids can further enhance the lubrication performance of the MQL technique. This aspect is inevitably closely related to the formation mechanism of the lubrication film on the abrasive grain/workpiece interface and its tribological properties.

In the following analyses, the formation mechanism of
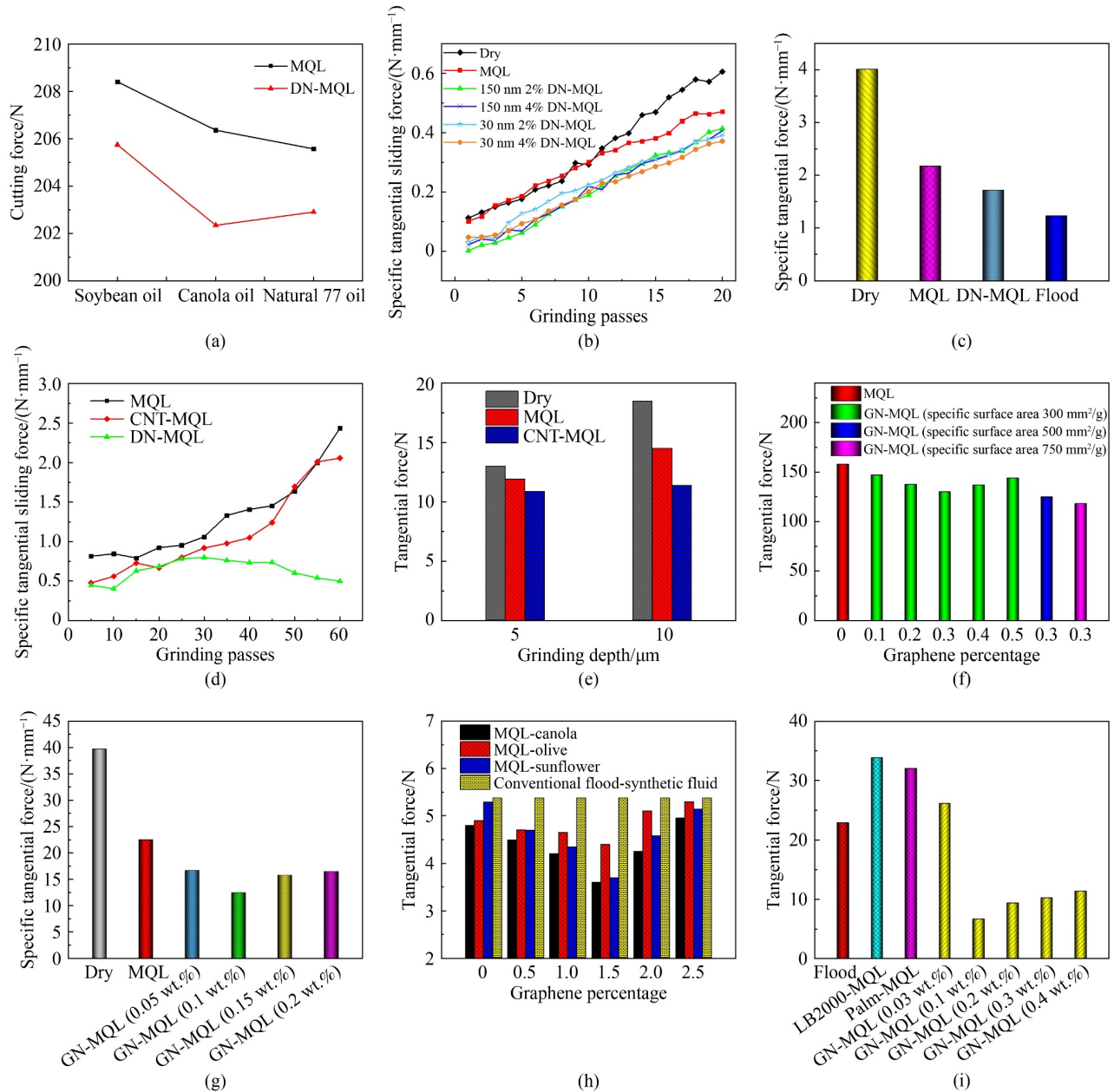
Fig. 10 Comparisons of experimental data: (a)–(c) between MQL and DN-MQL; (d) between MQL, DN-MQL, and CNT-MQL; (e) between MQL and CNT-MQL; (f)–(i) between MQL and GN-MQL.

the lubrication film generated by the [BMIM]BF$_4$ ionic liquid under the MQL condition is determined. Then, the tribological behaviors of the carbon group nanoparticles on the abrasive grain/workpiece interface are further investigated to reveal the tribological mechanisms of the carbon group nanofluids.

3.2 Formation mechanism of the lubrication film on the grain/workpiece interface under the MQL condition

Investigating the formation mechanism of the lubrication film under the MQL condition can pave the way for further revealing the tribological mechanisms of carbon group nanofluids on the abrasive grain/workpiece interface. The abovementioned analyses have established that tangential force can be significantly reduced by 16.9% under the MQL condition in contrast to that under dry grinding. This aspect is closely related to the presence of lubrication film on the abrasive grain/workpiece interface. The abrasive grain/workpiece contact states at the grinding distance of 6 nm under the MQL and dry grinding conditions are displayed in Fig. 11. Not only abrasive grain/workpiece contact areas but also non-contact areas can be observed under the MOL condition. On the non-contact areas, the ionic liquid molecules absorbed in the groove-like fractures on the grain wear's flat face form a lubrication film, separating the abrasive grain from the workpiece. According to tribology theory [54], the friction force F_f between the abrasive grain and the workpiece can be expressed as

$$F_f = \tau_s A_s + \tau_l A_l, \qquad (8)$$

where τ_s is the shear strength of the workpiece material, A_s is the contact area between the abrasive grain and workpiece, τ_l is the viscous resistance of the ionic liquid, and A_l is the action area of lubrication film.

Under the dry grinding condition, the groove-like fractures are filled with workpiece material (Fig. 11(a)). By contrast, under the MQL condition, ionic liquid molecules are stored in the groove-like fractures to form the lubrication film (Fig. 11(b)). The lubrication film can reduce the contact area A_s, thereby reducing the friction force F_f.

As further shown in Fig. 11(b), the cutting edge of the abrasive grain and the remaining areas on the wear's flat face (except the groove-like fractures) lack an adsorption film. This observation can be explained by the extremely

high extrusion stresses on these areas (Fig. 12). The ionic liquid molecules are extruded from the areas due to the high extrusion stresses. Hence, a boundary lubrication film is formed on the abrasive grain/workpiece interface. Fig. 13 shows the single-atom von Mises stress ranging from 27.5 to 206.6 MPa on the boundary lubrication region, in which the average von Mises stress is 126.4 MPa. The mechanical intensity of the boundary lubrication film can reach 126.4 MPa.

3.3 Tribological behaviors of carbon group nanoparticles on abrasive grain/workpiece interface

The aforementioned analyses indicate the ability of the ionic liquid to form a boundary lubrication film on the abrasive grain/workpiece interface under the MQL condition. Subsequently, the tribological behaviors of carbon group nanoparticles on the abrasive grain/workpiece interface are further investigated to reveal the tribological mechanisms of carbon group nanofluids on the MQL grinding interface.

3.3.1 Diamond nanofluid

On the basis of the aforementioned molecular dynamic simulations, under the DN-MQL condition, the tangential grinding force can be further reduced by 8.5% in contrast to that under the MQL condition. This scenario is closely
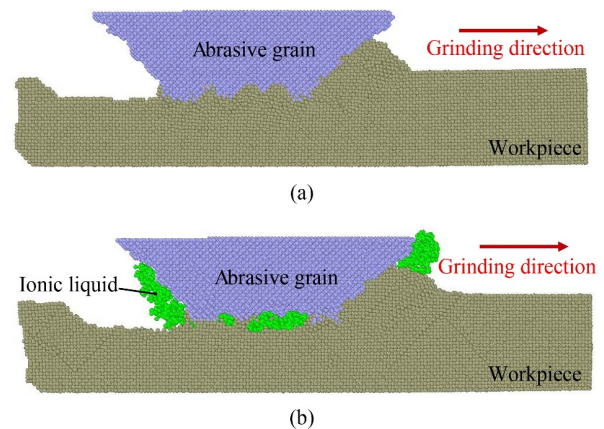
Fig. 11 Abrasive grain/workpiece contact states: (a) under dry and (b) MQL grinding conditions.
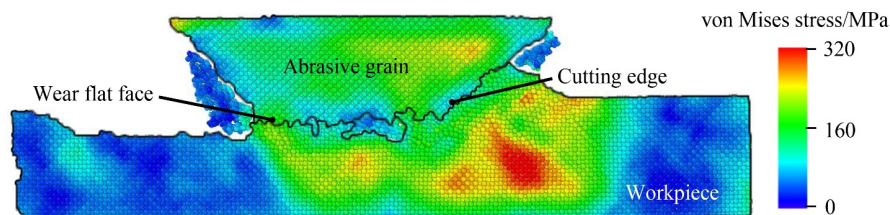
Fig. 12 von Mises stress distribution on the abrasive grain/workpiece interface.

related to the tribological behaviors of NDs on the abrasive grain/workpiece interface. Aimed at further analyzing the tribological behaviors, the initial state of the ND is marked, and its position is recorded within the grinding distance of 7 nm, as shown in Fig. 14, where S represents the grinding distance.

The tribological behavior of ND is dominated by rolling. Its total rotation angle is 493° within the grinding distance of 7 nm. When relative motion occurs between the abrasive grain and workpiece, NDs would roll on the interface because of their spherical structure and subsequently act as rolling balls. Thus, the sliding friction is transformed into rolling friction, reducing the tangential grinding force and further improving the tribological performance of the MQL technique.
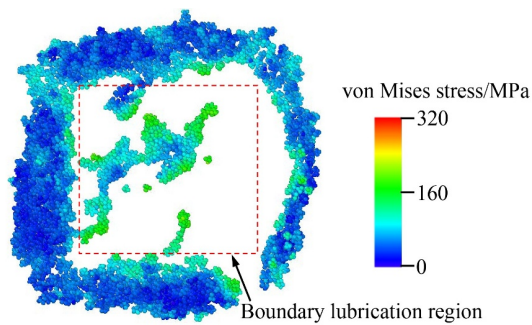
Fig. 13 Boundary lubrication region at the bottom of abrasive grains.

Here, the tribological behaviors of multi-nanoparticles are explored by increasing the number of diamond nanoparticles to five. The simulation results of the tangential grinding force are shown in Fig. 15. Compared with the findings for the single-diamond nanoparticle, the tangential grinding forces of the five-diamond nanoparticles are further reduced. This finding is mainly related to two factors. On the one hand, more diamond nanoparticles have a rolling effect on the abrasive grain/workpiece interface, and more sliding friction is transformed into rolling friction. On the other hand, the ionic liquid coating area on the interface is magnified by the increase in the number of diamond nanoparticles because of the polishing effect of the diamond nanoparticles [15,27,55] (Fig. 16). The combined effect of the two factors causes the tangential force of the five-diamond nanoparticles to further decrease compared with that of the single-diamond nanoparticle.

3.3.2 CNT nanofluid

Under the CNT-MQL condition, the tangential grinding force is further reduced by 12.0% in contrast to that under the MQL condition. This finding can also be obtained from the aforementioned simulations. Then, the tribological behaviors of CNTs on the abrasive grain/workpiece interface are revealed by marking the initial state of the CNT, and the position is recorded within the grinding distance of 7 nm, as shown in Fig. 17.
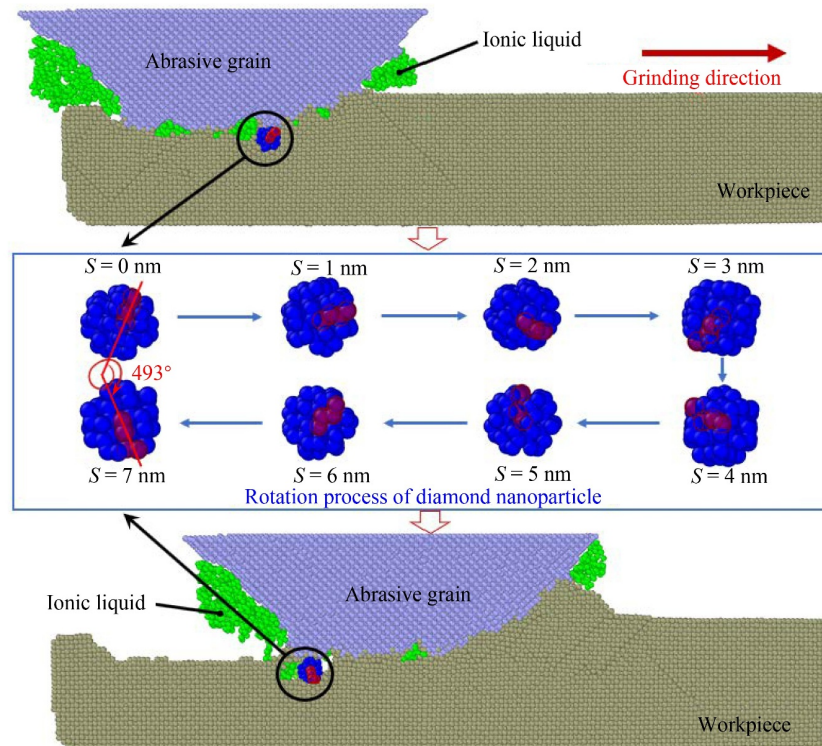
Fig. 14 Tribological behaviors of ND on the abrasive grain/workpiece interface.
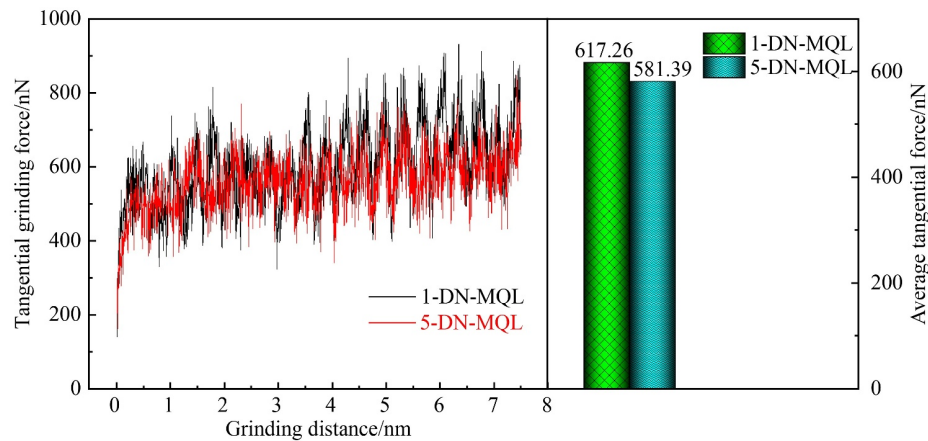
Fig. 15   Effect of the number of diamond nanoparticles on tangential grinding force.
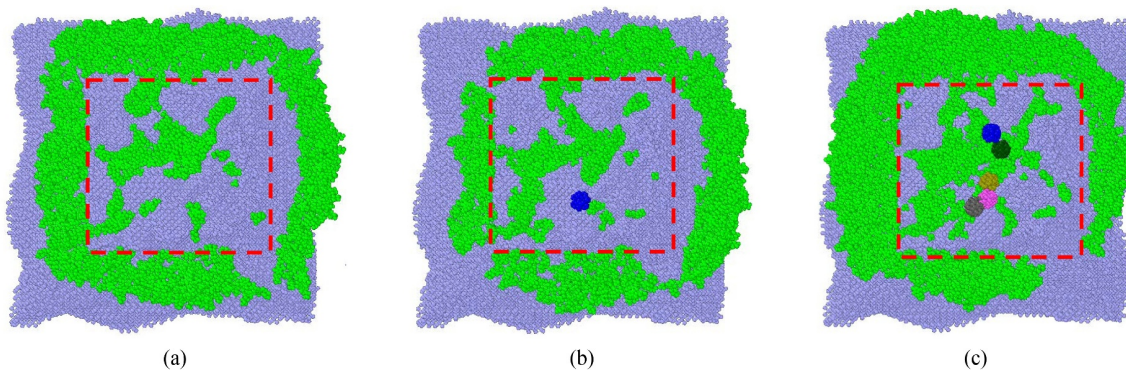
Fig. 16   Boundary lubrication status on the abrasive grain/workpiece grinding interface under (a) MQL, (b) 1-DN-MQL, and (c) 5-DN-MQL conditions.

Within the grinding distance range of 0–2 nm, the tribological behavior of CNT is mainly the sliding type. Within the grinding distance range of 2–7 nm, the rolling phenomenon is more obvious. Within the whole grinding distance of 0–7 nm, the total rotation angle of CNT is 478°, and its total sliding distance is 2.61 nm. Hence, the tribological behaviors of CNTs are both rolling and sliding on the abrasive grain/workpiece interface.

In the simulation (Fig. 17), the angle between CNT and grinding direction is close to 90°, as shown in Fig. 18(a). The influences of the rolling and sliding behaviors on the tangential grinding force are similarly analyzed via simulation, and the angle is close to 45° (Fig. 18(b)). This simulation indicates that the tribological behavior of CNT is completely sliding, as shown in Fig. 19.

The average tangential grinding forces under the MQL condition and the three CNT-MQL conditions are plotted in Fig. 20. Comparisons show that the minimum tangential force can be obtained under the CNT-MQL condition, with an angle close to 90°. Under this condition, both rolling and sliding occur on the abrasive grain/workpiece interface. By contrast, under the CNT-MQL condition, the angle is close to 45°. Although only sliding occurs on the interface, the tangential force is still reduced by 9.5% compared with that under the MQL condition. This finding indicates that the sliding effect also plays an important role on the friction-reducing performance of the CNT nanofluid.

In addition, CNTs have torsion behavior, which is related to their penetration position. As shown in Fig. 21(a), both ends of the CNT in the initial indentation state are in the groove-like fractures. The contact state of CNT at the bottom of the abrasive grain at the grinding distance of 2.5 nm is shown in Fig. 21(b). Both ends do not move relative to the abrasive grain despite the obstruction of the groove-like fractures. However, as presented in Fig. 21(c), a torsion of the CNT occurs due to the accumulation of the workpiece ahead of the CNT. Nonetheless, despite this torsion, the CNTs still manifest rolling and sliding behaviors, and the tangential grinding force is reduced by 10.0% compared with that under the MQL condition.

In summary, the tribological behaviors of CNTs are rolling and sliding on the abrasive grain/workpiece interface, and both of them play important roles in improving the tribological performance of the MQL technique. In addition, CNTs have torsion behavior, while torsional CNTs have rolling and sliding behaviors.

3.3.3 Graphene nanofluid

The aforementioned simulations show that the tangential grinding force under the GN-MQL condition can be further reduced by 14.1% compared with that under the MQL condition at the whole grinding distance. Subsequently, the tribological behaviors of GNs on the abrasive grain/workpiece interface are revealed by recording the morphological changes in the GN within the grinding distance of 7 nm (Fig. 22).

The grinding process under GN-MQL condition can be divided into two stages. The first stage is the grinding distance ranging from 0 to 4.5 nm, during which an interlayer shear effect occurs (Fig. 22(a)). At this stage, the tangential force under the GN-MQL condition decreases by 21.5% in contrast to that under the MQL condition (Fig. 23). This finding indicates that interlayer shear effect between neighboring layers can efficiently reduce the friction between the abrasive grain and workpiece. This phenomenon can be attributed to the layered structure of GNs and the low shearing strength between the neighboring layers. The second stage is the
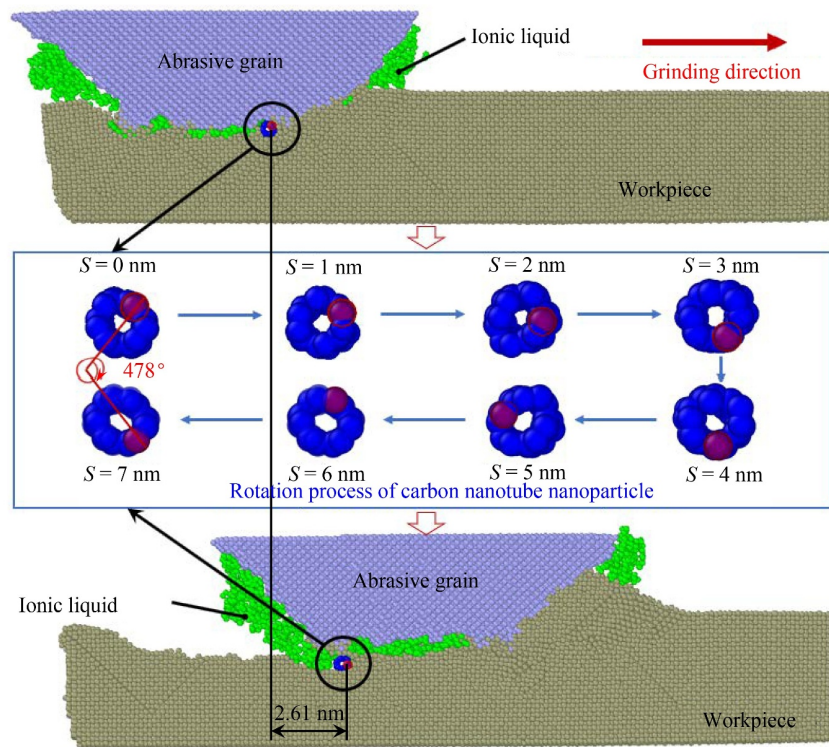
Fig. 17 Tribological behaviors of CNTs on the grain /workpiece interface.
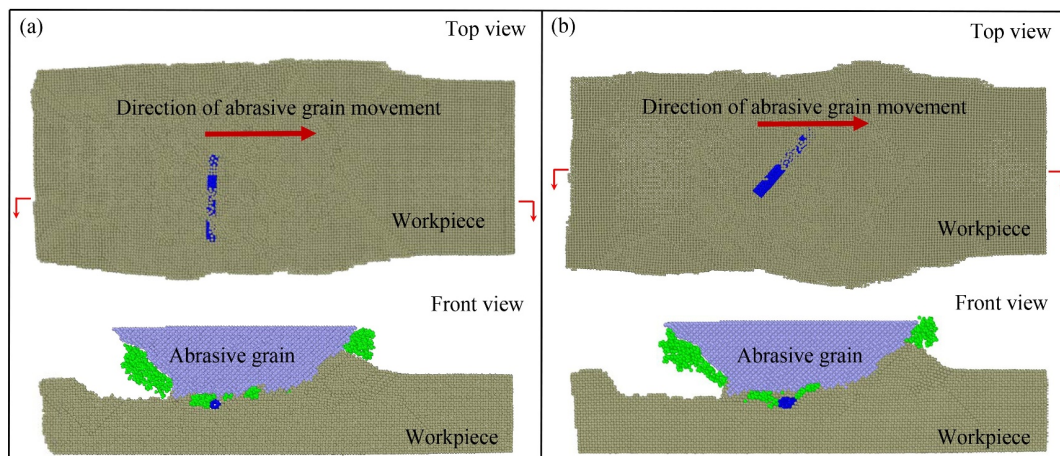
Fig. 18 Two different postures of CNTs: (a) nearly perpendicular to the grinding direction, and (b) leaning at an angle of about 45° to the grinding direction.
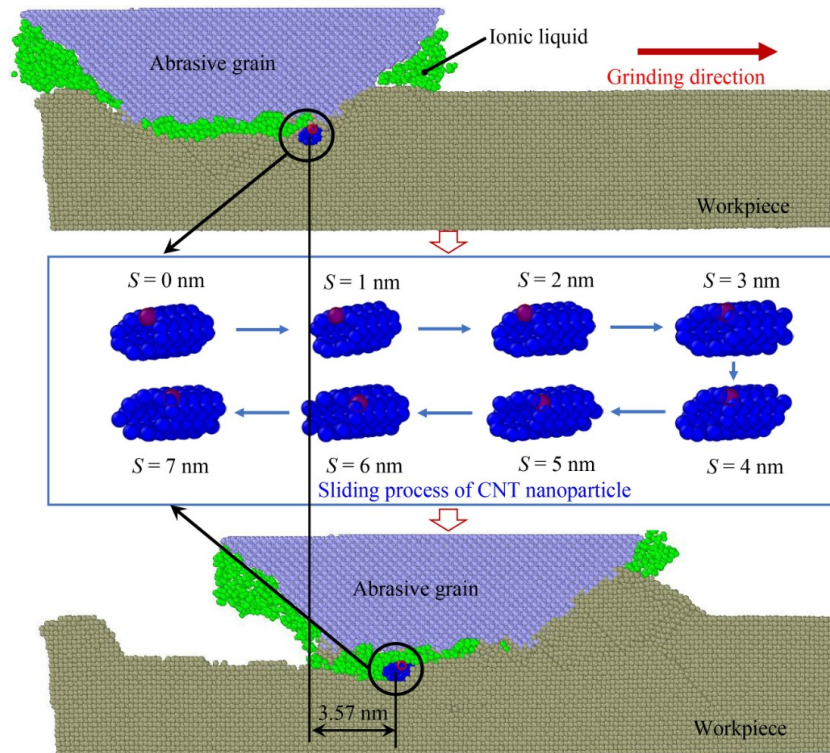
Fig. 19   Sliding effect of CNTs leaning at an angle of about 45° to the grinding direction.
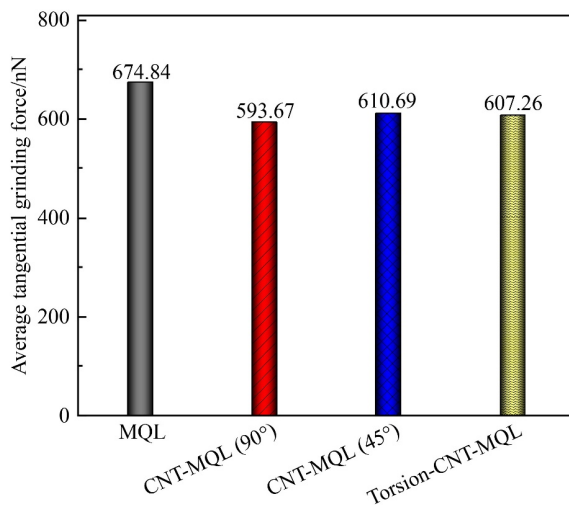
Fig. 20   Calculations of average tangential grinding forces under the MQL and CNT-MQL conditions.

grinding distance ranging from 4.5 to 7 nm, during which the interlayer shear effect is absent (Fig. 22(b)). At this stage, the tangential force under the GN-MQL condition is slightly different from that under the MQL condition (Fig. 23).

In conclusion, the tribological behavior of GNs is represented by the interlayer shear effect on the abrasive grain/workpiece interface, and it can further improve the lubrication performance of the MQL technique.

The top view of the workpiece-machined surface under

the GN-MQL condition depicts the tendency of GNs to adhere to the workpiece-machined surface (Fig. 24). This phenomenon can also be attained during grinding. Figure 25 presents the SEM and EDS analyses of the machined surface with graphene/ionic liquid nanofluid under the GN-MQL condition. Dark gray patches on the machined surface can be observed from the SEM images. Meanwhile, according to the EDS analyses, carbon elements gather within the patches in high density. Therefore, the dark gray patches are the GNs. This phenomenon is consistent with those found in the molecular dynamic simulations.

3.4   Effect area of carbon group nanoparticles on the abrasive grain/workpiece interface

Figure 26(a) presents the schematic diagram of the grain wear's flat face under the MQL condition. The acting position of ionic liquids and the direct contact region between the abrasive grain and workpiece are determined by color-coding of the abrasive grain at the bottom view along z axis (Figs. 26(b)–26(f)). Comparisons indicate that ionic liquids mainly act in the groove-like fractures on the grain wear's flat face, as shown by the light-blue region in Fig. 26(b), while the dark blue region represents the direct contact region between the abrasive grain and workpiece. Meanwhile, as shown in Figs. 26(c)–26(f), compared with trends under the MQL condition, carbon group nanoparticles mainly act on the direct contact
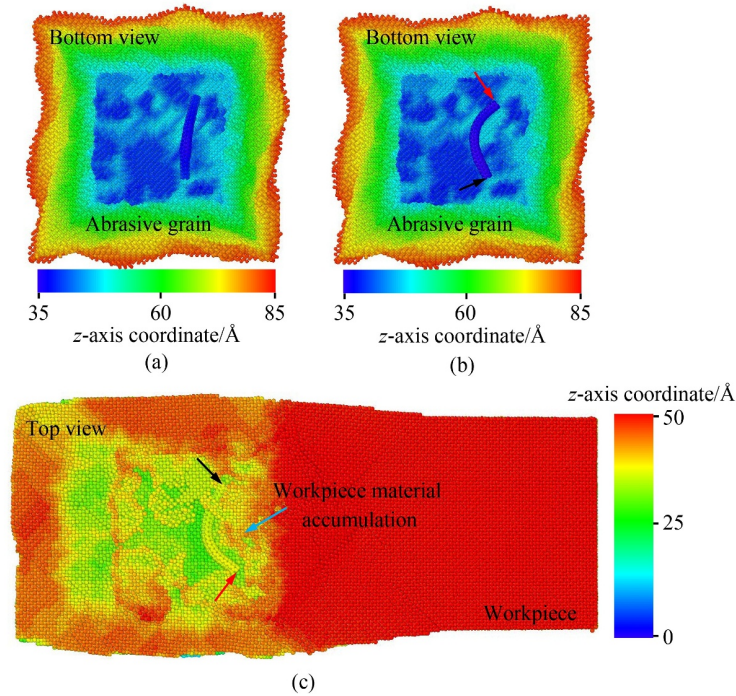
Fig. 21 Torsion behavior of CNT: (a) initial state, (b) bottom view of the abrasive grain at a grinding distance of 2.5 nm, and (c) top view of the workpiece-machined surface at a grinding distance of 2.5 nm.
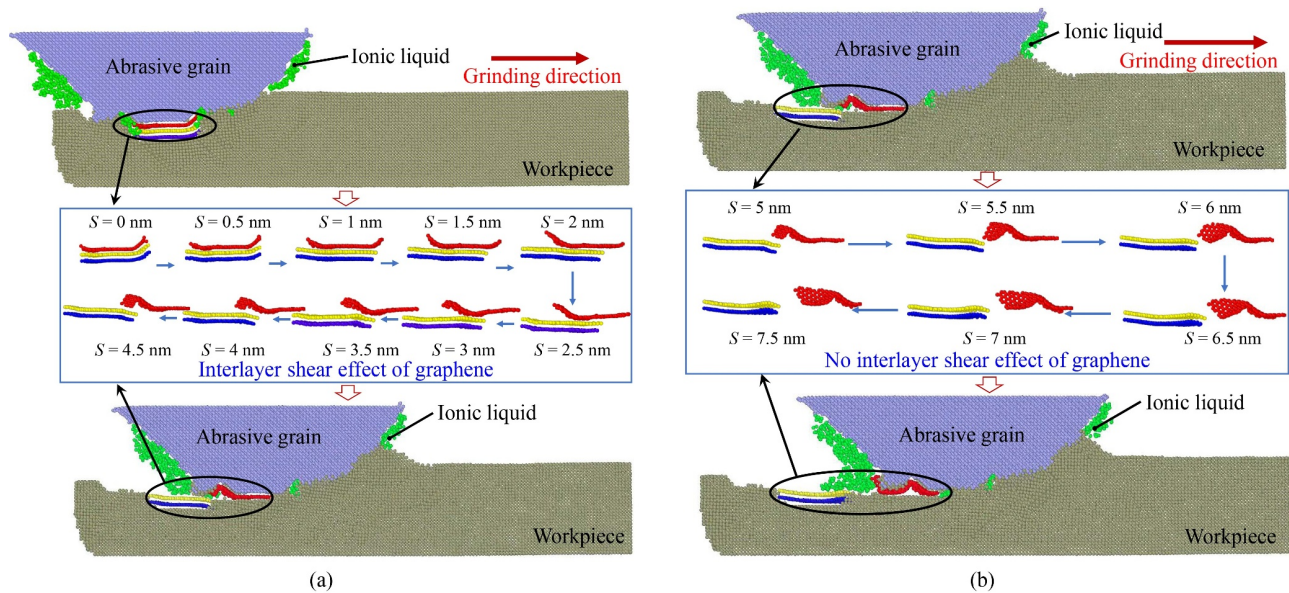
Fig. 22 Tribological behaviors of GNs on the abrasive grain/workpiece interface: (a) interlayer shear effect and (b) absence of the interlayer shear effect.

region, thereby reducing the contact area between the abrasive grain and workpiece. Nanoparticles will eventually manifest their corresponding tribological behaviors, such as sliding, rolling, and interlayer shearing, to reduce the tangential grinding force.

In accordance with the analyses of the tribological behaviors of the nanoparticles, the tribological mechanisms of the carbon group nanofluids on the MQL grinding interface can be summarized as follows. First, the ionic liquid base fluid is absorbed in the groove-like fractures on the grain wear's flat face to form a boundary lubrication film on the abrasive grain/workpiece interface. Then, the boundary lubrication film undergoes a friction-reducing effect by reducing the abrasive grain/workpiece contact area. Consequently, carbon group nanoparticles successfully enter the direct contact region between the
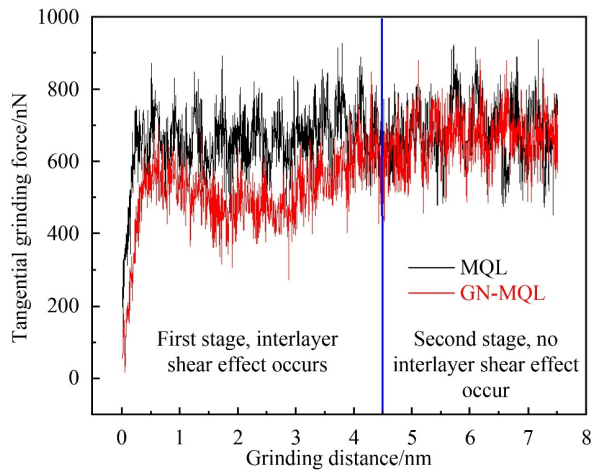
Fig. 23 Comparison of tangential grinding force histories.

abrasive grain and workpiece and enhance the lubrication performance on the abrasive grain/workpiece grinding

interface through their corresponding tribological behaviors. These behaviors involve the rolling effect of ND, rolling and sliding effects of CNT, and interlayer shear effect of GN.

4 Conclusions

Molecular dynamic simulations were performed to reveal the formation mechanism of the lubrication film generated by carbon group nanofluids on the MQL grinding interface, and diamond, CNT, and graphene nanofluids were taken as the representative specimens. The following conclusions can be drawn:

(1) Under the dry grinding condition, the abrasive grain directly comes into contact with the workpiece. The groove-like fractures on the grain wear's flat face are filled with the workpiece material to acquire the maximum tangential grinding force.
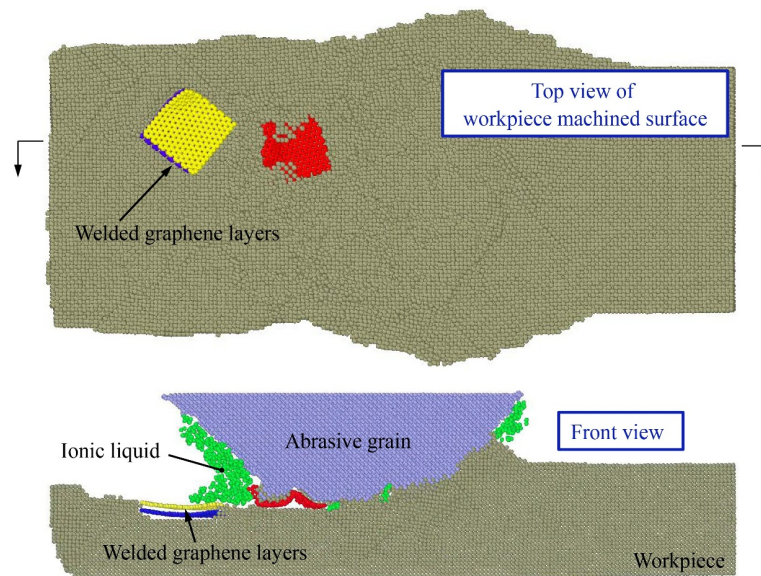
Fig. 24 Welding of graphene layers in the molecular dynamic simulation.
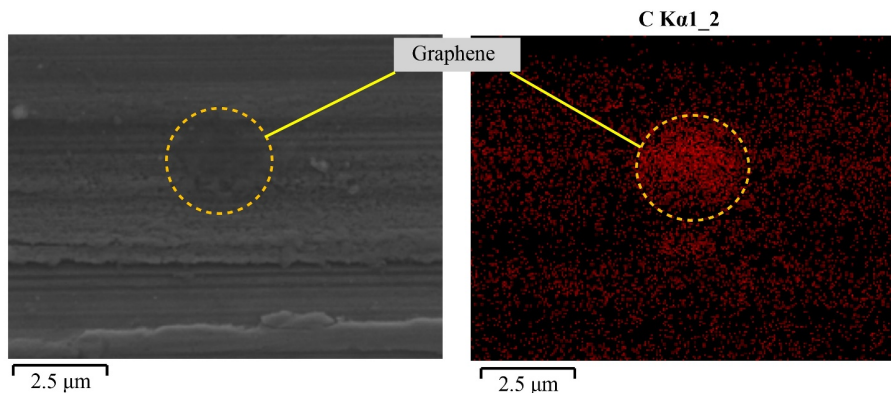
Fig. 25 SEM and EDS results of the workpiece-machined surface.
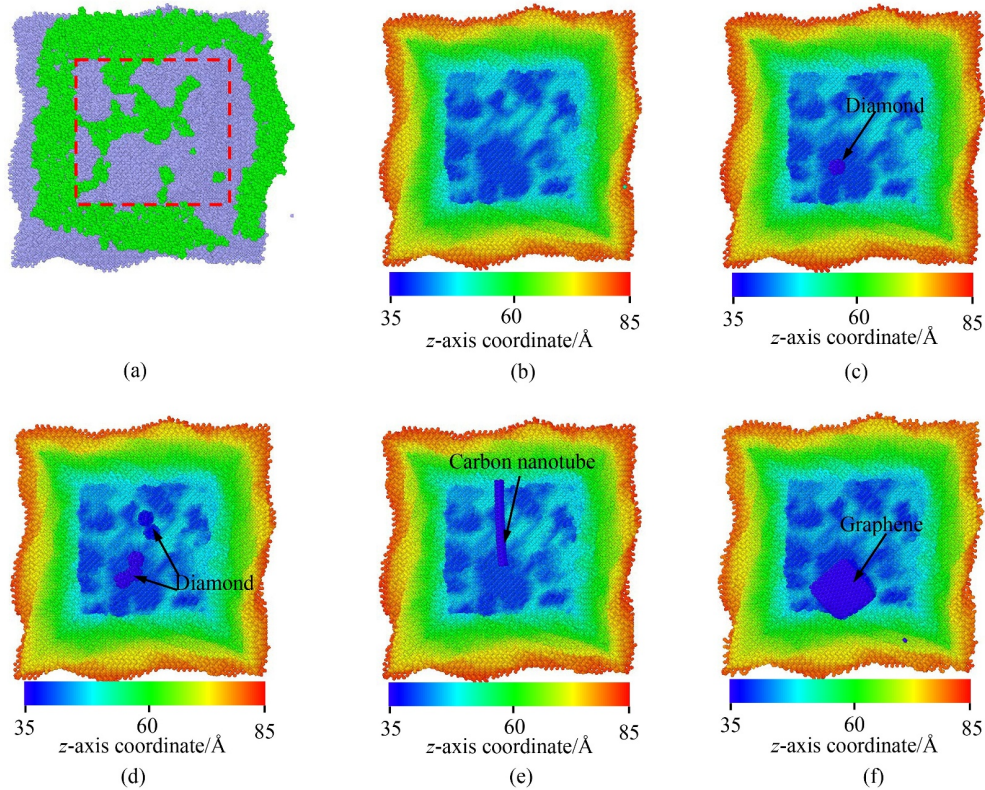
Fig. 26 Bottom views of the grain wear's flat face under (a)–(b) MQL, (c) 1-DN-MQL, (d) 5-DN-MQL, (e) CNT-MQL, and (f) GN-MQL conditions.

(2) Under the MQL condition, ionic liquid molecules are absorbed by the groove-like fractures to form a boundary lubrication film on the abrasive grain/workpiece interface. The lubrication film reduces the abrasive grain/workpiece contact area, lowering the tangential grinding force by 16.9% in contrast to that under dry grinding.

(3) Under the diamond nanofluid MQL condition, NDs roll on the abrasive grain/workpiece interface and act as rolling balls. The rolling effect transforms the sliding friction into rolling friction, further improving the tribological performance of the MQL technique. The tangential grinding force is further reduced by 8.5% in contrast to that under the MQL grinding condition.

(4) Under the CNT nanofluid MQL condition, the tribological behaviors of CNTs include rolling and sliding effects, both playing important roles in improving the tribological performance of the MQL technique.

(5) Under the graphene nanofluid MQL condition, the interlayer shear effect of GNs enhances the lubrication performance of the MQL technique. During the grinding stage in which the interlayer shear effect occurs, the tangential force decreases by 21.5% in contrast to that under the MQL condition. By contrast, at the stage in which no interlayer shear effect occurs, the tangential force somewhat differs from that under the MQL condition.

Nomenclature

Abbreviations

CBN	Cubic boron nitride
CFRP	Carbon fiber-reinforced polymer
CNT	Carbon nanotube
CNT-MQL	Carbon nanotube nanofluid minimum quantity lubrication
DN-MQL	Diamond nanofluid minimum quantity lubrication
EDS	Energy dispersive spectrometer
GN	Graphene nanosheet
GN-MQL	Graphene nanofluid minimum quantity lubrication
LJ	Lennard–Jones
MQL	Minimum quantity lubrication
MWCNT	Multi-walled carbon nanotube
ND	Nanodiamond
NMQL	Nanofluid minimum quantity lubrication
SEM	Scanning electron microscope

Variables

A_l	Action area of lubricating film
A_s	Contact area between abrasive grain and workpiece
D	Binding energy coefficient

E	Total energy
F	Embedding energy
F_f	Frictional force
K_r	Bond-stretching energy coefficient
K_θ	Bond angle-bending energy coefficient
K_ϕ	Torsion energy coefficient
n	Multiphase factor
N	Total amount of atoms in the system
q_i, q_j	Electrical charges of the atoms i and j, respectively
r	Bond length
r_0	Equilibrium bond length
r_{ij}	Distance between atoms i and j
R	Pair interactions
t_i	Chemical species (Fe, Ni, or Cr)
V	Volume of the sphere
α	Gradient coefficient of potential energy curve
γ	Equilibrium dihedral angle
ε_{ij}	Traditional well-depth
θ	Bond angle
θ_0	Equilibrium bond angle
ρ_i	Local electron density around atom i
σ_{ij}	Distance between atoms i and j
σ_v	von Mises equivalent stress
τ_l	Viscous resistance of ionic liquid
τ_s	Shear strength of workpiece material

References

1. Sánchez J A, Pombo I, Alberdi R, Izquierdo B, Ortega N, Plaza S, Martinez-Toledano J. Machining evaluation of a hybrid MQL-CO_2 grinding technology. Journal of Cleaner Production, 2010, 18: 1840–1849

2. Hamran N N N, Ghani J A, Ramli R, Che Haron C H. A review on recent development of minimum quantity lubrication for sustainable machining. Journal of Cleaner Production, 2020, 268: 122165

3. Jia D Z, Li C H, Zhang D K, Wang S, Hou Y L. Investigation into the formation mechanism and distribution characteristics of suspended microparticles in MQL grinding. Recent Patents on Mechanical Engineering, 2014, 7(1): 52–62

4. Yin Q A, Li C H, Dong L, Bai X F, Zhang Y B, Yang M, Jia D Z, Li R Z, Liu Z Q. Effects of physicochemical properties of different base oils on friction coefficient and surface roughness in MQL milling AISI 1045. International Journal of Precision Engineering and Manufacturing-Green Technology, 2021, 8(6): 1629–1647

5. Stachurski W, Sawicki J, Januszewicz B, Rosik R. The influence of the depth of grinding on the condition of the surface layer of 20MnCr5 steel ground with the minimum quantity lubrication (MQL) method. Materials, 2022, 15(4): 1336

6. Hadad M, Sadeghi B. Thermal analysis of minimum quantity lubrication-MQL grinding process. International Journal of Machine Tools and Manufacture, 2012, 63: 1–15

7. Zhang J C, Wu W T, Li C H, Yang M, Zhang Y B, Jia D Z, Hou Y L, Li R Z, Cao H J, Ali H M. Convective heat transfer coefficient model under nanofluid minimum quantity lubrication coupled with cryogenic air grinding Ti–6Al–4V. International Journal of Precision Engineering and Manufacturing-Green Technology, 2021, 8(4): 1113–1135

8. Tawakoli T, Hadad M J, Sadeghi M H. Influence of oil mist parameters on minimum quantity lubrication—MQL grinding process. International Journal of Machine Tools and Manufacture, 2010, 50(6): 521–531

9. Zhang X Z, Huang W, Liu Q G. Heat Transfer Theory. Beijing: National Defense Industry Press, 2011 (in Chinese)

10. Pimenov D Y, Mia M, Gupta M K, Machado A R, Tomaz Í V, Sarikaya M, Wojciechowski S, Mikolajczyk T, Kapłonek W. Improvement of machinability of Ti and its alloys using cooling-lubrication techniques: a review and future prospect. Journal of Materials Research and Technology, 2021, 11: 719–753

11. Nwoguh T O, Okafor A C, Onyishi H A. Enhancement of viscosity and thermal conductivity of soybean vegetable oil using nanoparticles to form nanofluids for minimum quantity lubrication machining of difficult-to-cut metals. The International Journal of Advanced Manufacturing Technology, 2021, 113(11–12): 3377–3388

12. Sui M H, Li C H, Wu W T, Yang M, Ali H M, Zhang Y B, Jia D Z, Hou Y L, Li R Z, Cao H J. Temperature of grinding carbide with castor oil-based MoS_2 nanofluid minimum quantity lubrication. Journal of Thermal Science and Engineering Applications, 2021, 13(5): 051001

13. Li B K, Li C H, Zhang Y B, Wang Y G, Jia D Z, Yang M, Zhang N Q, Wu Q D, Han Z G, Sun K. Heat transfer performance of MQL grinding with different nanofluids for Ni-based alloys using vegetable oil. Journal of Cleaner Production, 2017, 154: 1–11

14. Chinchanikar S, Kore S S, Hujare P. A review on nanofluids in minimum quantity lubrication machining. Journal of Manufacturing Processes, 2021, 68: 56–70

15. Zhang Y B, Li H N, Li C H, Huang C Z, Ali H M, Xu X F, Mao C, Ding W F, Cui X, Yang M, Yu T B, Jamil M, Gupta M K, Jia D Z, Said Z. Nano-enhanced biolubricant in sustainable manufacturing: from processability to mechanisms. Friction, 2022, 10(6): 803–841

16. Virdi R L, Chatha S S, Singh H. Experiment evaluation of grinding properties under Al_2O_3 nanofluids in minimum quantity lubrication. Materials Research Express, 2019, 6(9): 096574

17. Virdi R L, Chatha S S, Singh H. Performance evaluation of nanofluid-based minimum quantity lubrication grinding of Ni–Cr alloy under the influence of CuO nanoparticles. Advances in Manufacturing, 2021, 9(4): 580–591

18. Zhang Z C, Sui M H, Li C H, Zhou Z M, Liu B, Chen Y, Said Z,

Debnath S, Sharma S. Residual stress of grinding cemented carbide using MoS$_2$ nano-lubricant. The International Journal of Advanced Manufacturing Technology, 2022, 119(9–10): 5671–5685

19. Dambatta Y S, Sayuti M, Sarhan A A D, Hamdi M, Manladan S M, Reddy M. Tribological performance of SiO$_2$-based nanofluids in minimum quantity lubrication grinding of Si$_3$N$_4$ ceramic. Journal of Manufacturing Processes, 2019, 41: 135–147

20. Pashmforoush F, Delir Bagherinia R. Influence of water-based copper nanofluid on wheel loading and surface roughness during grinding of Inconel 738 superalloy. Journal of Cleaner Production, 2018, 178: 363–372

21. Prabu L, Saravanakumar N, Rajaram G. Influence of Ag nanoparticles for the anti-wear and extreme pressure properties of the mineral oil based nano-cutting fluid. Tribology in Industry, 2018, 40(3): 440–447

22. Hegab H, Kishawy H A, Gadallah M H, Umer U, Deiab I. On machining of Ti–6Al–4V using multi-walled carbon nanotubes-based nano-fluid under minimum quantity lubrication. The International Journal of Advanced Manufacturing Technology, 2018, 97(5–8): 1593–1603

23. Gao T, Li C H, Jia D Z, Zhang Y B, Yang M, Wang X M, Cao H J, Li R Z, Ali H M, Xu X F. Surface morphology assessment of CFRP transverse grinding using CNT nanofluid minimum quantity lubrication. Journal of Cleaner Production, 2020, 277: 123328

24. Gao T, Zhang X P, Li C H, Zhang Y B, Yang M, Jia D Z, Ji H J, Zhao Y J, Li R Z, Yao P, Zhu L D. Surface morphology evaluation of multi-angle 2D ultrasonic vibration integrated with nanofluid minimum quantity lubrication grinding. Journal of Manufacturing Processes, 2020, 51: 44–61

25. de Paiva R L, de Souza Ruzzi R, de Oliveira L R, Bandarra Filho E P, Gonçalves Neto L M, Gelamo R V, da Silva R B. Experimental study of the influence of graphene platelets on the performance of grinding of SAE 52100 steel. The International Journal of Advanced Manufacturing Technology, 2020, 110(1–2): 1–12

26. Lee P H, Nam T S, Li C J, Lee S W. Environmentally-friendly nano-fluid minimum quantity lubrication (MQL) meso-scale grinding process using nano-diamond particles. In: Proceedings of 2010 International Conference on Manufacturing Automation, 2010, 44–49

27. Wang Y G, Li C H, Zhang Y B, Li B K, Yang M, Zhang X P, Guo S M, Liu G T. Experimental evaluation of the lubrication properties of the wheel/workpiece interface in MQL grinding with different nanofluids. Tribology International, 2016, 99: 198–210

28. Lee P H, Nam J S, Li C J, Lee S W. An experimental study on micro-grinding process with nanofluid minimum quantity lubrication (MQL). International Journal of Precision Engineering and Manufacturing, 2012, 13(3): 331–338

29. Shen B, Shih A J, Tung S C. Application of nanofluids in minimum quantity lubrication grinding. Tribology Transactions, 2008, 51(6): 730–737

30. Kumar M K, Ghosh A. On grinding force ratio, specific energy, G-ratio and residual stress in SQCL assisted grinding using aerosol of MWCNT nanofluid. Machining Science and Technology, 2021, 25(4): 585–607

31. Huang W T, Liu W S, Wu D H. Investigations into lubrication in grinding processes using MWCNTs nanofluids with ultrasonic-assisted dispersion. Journal of Cleaner Production, 2016, 137: 1553–1559

32. Gao T, Li C H, Yang M, Zhang Y B, Jia D Z, Ding W F, Debnath S, Yu T B, Said Z, Wang J. Mechanics analysis and predictive force models for the single-diamond grain grinding of carbon fiber reinforced polymers using CNT nano-lubricant. Journal of Materials Processing Technology, 2021, 290: 116976

33. Singh H, Sharma V S, Dogra M. Exploration of graphene assisted vegetables oil based minimum quantity lubrication for surface grinding of Ti–6Al–4V-ELI. Tribology International, 2020, 144: 106113

34. Li M, Yu T B, Zhang R C, Yang L, Ma Z L, Li B C, Wang X Z, Wang W S, Zhao J. Experimental evaluation of an eco-friendly grinding process combining minimum quantity lubrication and graphene-enhanced plant-oil-based cutting fluid. Journal of Cleaner Production, 2020, 244: 118747

35. De Oliveira D, Da Silva R B, Gelamo R V. Influence of multilayer graphene platelet concentration dispersed in semi-synthetic oil on the grinding performance of Inconel 718 alloy under various machining conditions. Wear, 2019, 426–427, Part B: 1371–1383

36. Singh A K, Kumar A, Sharma V, Kala P. Sustainable techniques in grinding: state of the art review. Journal of Cleaner Production, 2020, 269: 121876

37. Ren J, Hao M R, Lv M, Wang S Y, Zhu B Y. Molecular dynamics research on ultra-high-speed grinding mechanism of monocrystalline nickel. Applied Surface Science, 2018, 455: 629–634

38. Doan D Q, Fang T H, Chen T H. Nanomachining characteristics of textured polycrystalline NiFeCo alloy using molecular dynamics. Journal of Manufacturing Processes, 2022, 74: 423–440

39. Peng R T, Tong J W, Zhao L F, Tang X Z, Peng X, He X B. Molecular dynamics study on the adsorption synergy of MWCNTs/MoS$_2$ nanofluids and its influence of internal-cooling grinding surface integrity. Applied Surface Science, 2021, 563: 150312

40. Wang D X, Sun S F, Tang Y Z, Liu X F, Jiang J L. Molecular dynamics simulation for grinding interface under minimum quantity lubrication. Journal of Xi'an Jiaotong University, 2020, 54(12): 168–175 (in Chinese)

41. Fan Y H, Wang W Y, Hao Z P, Zhan C Y. Work hardening mechanism based on molecular dynamics simulation in cutting Ni–Fe–Cr series of Ni-based alloy. Journal of Alloys and Compounds, 2020, 819: 153331

42. Los J H, Kroes J M H, Albe K, Gordillo R M, Katsnelson M I, Fasolino A. Extended Tersoff potential for boron nitride: energetics and elastic properties of pristine and defective h-BN. Physical Review B, 2017, 96(18): 184108

43. Bonny G, Terentyev D, Pasianot R C, Poncé S, Bakaev A. Interatomic potential to study plasticity in stainless steels: the FeNiCr model alloy. Modelling and Simulation in Materials Science and Engineering, 2011, 19(8): 085008

44. Liu Z P, Huang S P, Wang W C. A refined force field for molecular simulation of imidazolium-based ionic liquids. The Journal of Physical Chemistry B, 2004, 108(34): 12978–12989

45. Tersoff J. Empirical interatomic potential for silicon with improved

elastic properties. Physical Review B, 1988, 38(14): 9902–9905

46. Chang X. Ripples of multilayer graphenes: a molecular dynamics study. Acta Physica Sinica, 2014, 63(8): 086102

47. Hao Z P, Cui R R, Fan Y H, Lin J Q. Diffusion mechanism of tools and simulation in nanoscale cutting the Ni–Fe–Cr series of Nickel-based superalloy. International Journal of Mechanical Sciences, 2019, 150: 625–636

48. Liang T, Zhang P, Yuan P, Zhai S P. In-plane thermal transport in black phosphorene/graphene layered heterostructures: a molecular dynamics study. Physical Chemistry Chemical Physics, 2018, 20(32): 21151–21162

49. Wang D X, Zhao Q L, Zhang Y, Gao T, Jiang J L, Liu G L, Li C H. Investigation on tribological mechanism of ionic liquid on grinding interfaces under MQL. China Mechanical Engineering, 2022, 33(5): 560–568, 606 (in Chinese)

50. Yuan S M, Hou X B, Wang L, Chen B C. Experimental investigation on the compatibility of nanoparticles with vegetable oils for nanofluid minimum quantity lubrication machining. Tribology Letters, 2018, 66(3): 106

51. Jia D Z, Li C H, Zhang D K, Zhang Y B, Zhang X W.

Experimental verification of nanoparticle jet minimum quantity lubrication effectiveness in grinding. Journal of Nanoparticle Research, 2014, 16(12): 2758

52. Pavan R B, Venu Gopal A, Amrita M, Goriparthi B K. Experimental investigation of graphene nanoplatelets-based minimum quantity lubrication in grinding Inconel 718. Proceedings of the Institution of Mechanical Engineers, Part B: Journal of Engineering Manufacture, 2019, 233(2): 400–410

53. Ibrahim A M M, Li W, Xiao H, Zeng Z X, Ren Y H, Alsoufi M S. Energy conservation and environmental sustainability during grinding operation of Ti–6Al–4V alloys via eco-friendly oil/graphene nano additive and minimum quantity lubrication. Tribology International, 2020, 150: 106387

54. Moore D F. Principles and Applications of Tribology. Pergamon: Elsevier, 1975

55. Wang Y G, Li C H, Zhang Y B, Li B K, Yang M, Zhang X P, Guo S M, Liu G T, Zhai M G. Comparative evaluation of the lubricating properties of vegetable-oil-based nanofluids between frictional test and grinding experiment. Journal of Manufacturing Processes, 2017, 26: 94–104